Physiological and functional heterogeneity in the mouse locus coeruleus

Running title: Heterogeneity in the locus coeruleus

Lucas Silva Tortorelli[1 *], Jim McBurney-Lin[1,2 *], Machhindra Garad[1], Marine Megemont[1], Martin Riccomagno[1,2] and Hongdian Yang[1,2]

[1] Department of Molecular, Cell and Systems Biology, [2] Neuroscience Graduate Program, University of California, Riverside, CA 92521, USA

[*] Equal contributions

Correspondence: hongdian@ucr.edu

Keywords: heterogeneity, locus coeruleus, mouse, pupil diameter

Abstract

Neurons in the locus coeruleus (LC) have been traditionally viewed as a homogenous population. Recent studies are beginning to uncover heterogeneous molecular phenotypes and projection targets in this nucleus, but how such heterogeneity is ultimately manifested in neuronal physiology and function is largely unknown. We took an orthogonal approach to directly assess the physiological and functional heterogeneity in the LC. By identifying noradrenergic neurons using a genetic-based tagging approach, our study revealed a subset of neurons exhibiting a distinctive narrow spike waveform and lacking the prolonged after-hyperpolarization. We further provided evidence establishing a link between the proximity of LC neurons and their response latency, where putatively proximal neurons tended to have a long latency to optogenetic activation. Finally, we found that response latency of LC neurons was correlated with their burst firing and distinct relationship with pupil diameter. Together, our study presents novel evidence to reveal and link LC heterogeneity at the physiological level to that at the functional level.

Introduction

The noradrenergic nucleus locus coeruleus (LC) is interconnected with many regions in the nervous system, and has been implicated in a multitude of physiological and cognitive functions ranging from sleep-wake cycle and sensory perception to attention and memory (Berridge and Waterhouse, 2003; Aston-Jones and Cohen, 2005; Sara and Bouret, 2012; McBurney-Lin et al., 2019). Neurons in the LC have been traditionally viewed as a uniform population with homogenous intrinsic properties and functions (Aston-Jones and Bloom, 1981; Fallon and Loughlin, 1982; Loughlin et al., 1982; Waterhouse et al., 1993). Recent advances in single cell profiling and tracing (e.g., (Macosko et al., 2015; Shekhar et al., 2016; Tervo et al., 2016; Zingg et al., 2020)) have revealed heterogeneity in neuronal populations that were once thought to be homogeneous. These approaches have also begun to challenge the longstanding view of homogeneity in the LC (Chandler et al., 2019; Poe et al., 2020), uncovering heterogeneity at multiple levels including developmental origins, molecular phenotypes and projection targets (Robertson et al., 2013; Chandler et al., 2014; Schwarz et al., 2015; Kebschull et al., 2016; Kempadoo et al., 2016; Hirschberg et al., 2017; Plummer et al., 2017; Uematsu et al., 2017; Mulvey et al., 2018; Borodovitsyna et al., 2020). However, how heterogeneity at the subcellular and anatomical level is ultimately manifested in LC physiology and function is largely unknown and is under active investigation. In addition, one widely adopted criterion to identify LC neurons *in vivo* relies on their distinctive wide spike waveforms with prolonged after-hyperpolarization (e.g., (Andrade and Aghajanian, 1984; Berridge and Waterhouse, 2003)). Since 'blind' *in vivo* recordings cannot determine cellular identity, i.e., whether the recorded neurons are indeed noradrenergic-positive (NA+), such inclusion criteria may be biased to sample a subpopulation of neurons. It is currently unclear whether LC NA+ neurons ubiquitously exhibit wide spike waveforms (Totah et al., 2018; Breton-Provencher and Sur, 2019). More importantly, it is currently unknown whether and how LC physiological diversity underlies any heterogeneity at the functional level.

Deeply situated in the brainstem, the LC poses a great technical challenge for *in vivo* recordings. Based on anatomical structures and empirical measurements (Breen et al., 1983; Rajkowski et al., 1994; Murphy et al., 2014; Varazzani et al., 2015; Reimer et al., 2016; Liu et al., 2017; Breton-Provencher and Sur, 2019; Privitera et al., 2020), pupil diameter has been widely treated as a noninvasive readout of LC activity (e.g., (Aston-Jones and Cohen, 2005; Gilzenrat et al., 2010; Preuschoff et al., 2011; Clewett et al., 2020)). This view has also been challenged by recent findings that pupil size changes correlate with activity in other brain structures, and that pupil and LC respond to task epochs differently and have variable relationships (Joshi et al., 2016; Cazettes

et al., 2020; Yang et al., 2021; Megemont et al., 2022). However, it is still unclear whether physiological diversity of LC neurons contributes to their distinct relationship with pupil diameter. Elucidating heterogeneity in the pupil-LC relationship will provide mechanistic insights into and set appropriate constraints on interpreting pupil diameter as a readout of LC activity.

To address these questions, we took advantage of recent development in mouse genetics that allowed identifying NA+ neurons with a specific marker, i.e., the presence of dopamine-beta-hydroxylase (DBH, an enzyme in the NA synthesize pathway downstream of tyrosine hydroxylase), and expressed ChannelRhodopsin-2 (ChR2) in DBH+ neurons. We recorded spiking activity from single units in the LC that were responsive to optogenetic stimulation, with a subset of these units exhibiting a distinctive narrow spike waveform and lacking the prolonged after-hyperpolarization. A fraction, but not all of the narrow units appeared to be fast spiking. Next, we provided evidence revealing a link between the proximity of LC neurons and their response latency, where putatively spatially proximal neurons tended to have a long latency in response to optogenetic activation. Finally, we found that response latency of LC neurons was correlated with their burst firing and distinct relationship with pupil diameter. Together, this study presents novel evidence to advance our understanding of the heterogeneity of LC neurons at the functional level, and provides further physiological insights into the relationship between pupil and LC.

Results

To collect a dataset that consisted of putatively noradrenergic neurons in the LC, we implemented an approach to drive a genetically encoded ChannelRhodopsin-2 (ChR2(H134R)) transgene monoallelically from the *Gt(ROSA)26Sor* locus (*DBH-Cre/+;Ai32/+*). Taking this approach instead of using a viral vector should allow less variation in copy number and spatial spread when expressing ChR2 across DBH+ neurons. We used long pulses (0.2-0.3 s) for optogenetic tagging as recent work showed that a subset of LC neurons cannot be excited by short pulses (Hickey et al., 2014; Li et al., 2016). Only neurons that emitted spikes in response to optogenetic stimulation were included in the dataset (Fig. 1a, b).

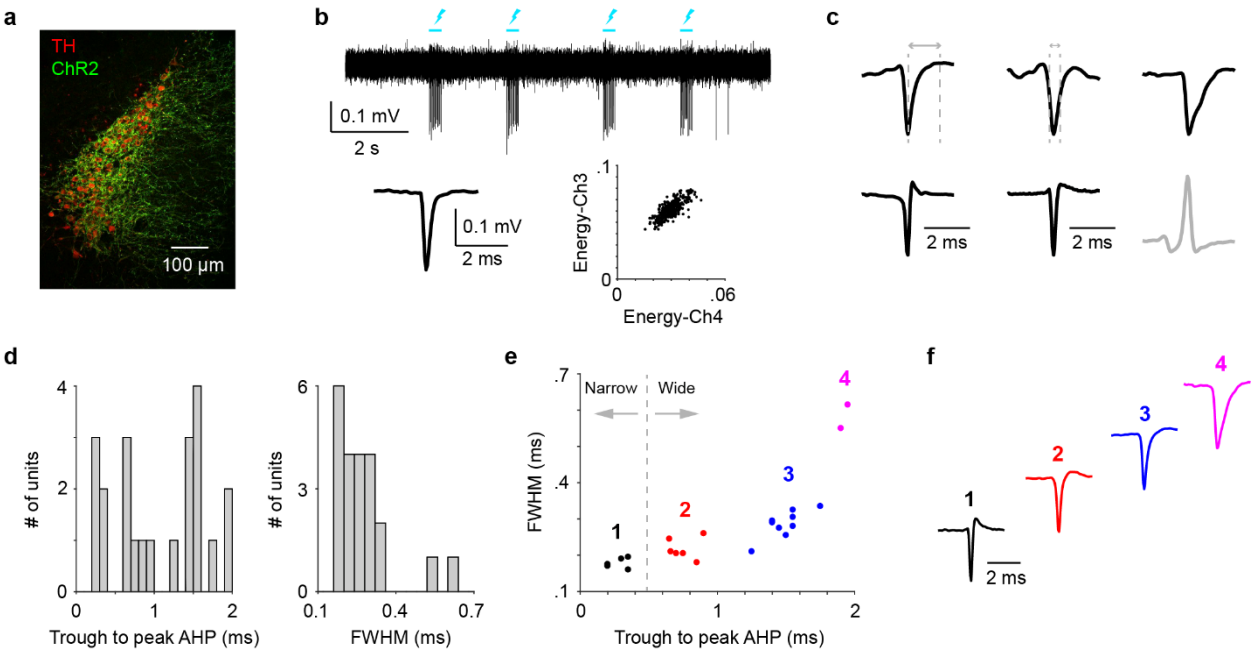

Figure 1. Quantifying spike waveforms of the units

(a) ChR2 expression in a DBH-Cre/+;Ai32/+ mouse. TH: Tyrosine hydroxylase.

(b) Top: Response of a ChR2-expressing LC neuron to optogenetic stimulation (lightning bolts). Bottom: Spike waveform and spike sorting diagram of this unit.

(c) Example spike waveforms with trough to peak AHP and FWHM indicated. Black: typical extracellular spike waveforms with negative-positive polarity. Gray: Spike waveforms with distorted/reversed polarity. Only units with the typical waveforms were included in d-f.

(d) Histogram of trough to peak AHP (Left) and FWHM (Right) of LC units (n = 22).

(e) Scatter plot of trough to peak AHP vs. FWHM, based on which K-means clustering classified 4 classes of spike waveforms (color coded).

(f) Average spike waveform of each class in (e).

We first reported spike waveform properties of these neurons (35 units from 26 recordings of 21 mice). We strove to ensure that all units were distinct from one another by taking a conservative approach to include one recording from each mouse, with one exception: when a second recording from the same animal was acquired on a separate day, and a light-responsive unit was present in a tetrode channel different from the first recording, the unit from the second recording was considered distinct from the first recording and included (5 units from the second recordings of 5 mice. Waveform similarity between units from the second recording and units from the first recording of the same mouse: 0.35 ± 0.23, mean ± SEM, Methods). Typically, we were able to

sort one single unit from a recording (18/26 (69%) recordings yielded 18 units), but a subset of recordings yielded multiple tagged units (8/26 (31%) recordings yielded 17 units). We observed a spectrum of spike waveforms from this dataset, the majority of which had the typical polarity of extracellularly recorded waveform (negative-positive polarity, 22/35. Fig.1c black). A minority exhibited distorted/reversed polarity (13/35. Fig. 1c gray), indicating that the recording site was in the distal axonal or dendritic compartment of a neuron where estimating waveform properties would be less accurate (Rall and Shepherd, 1968; Gold et al., 2006; Barry, 2015; Sun et al., 2021).

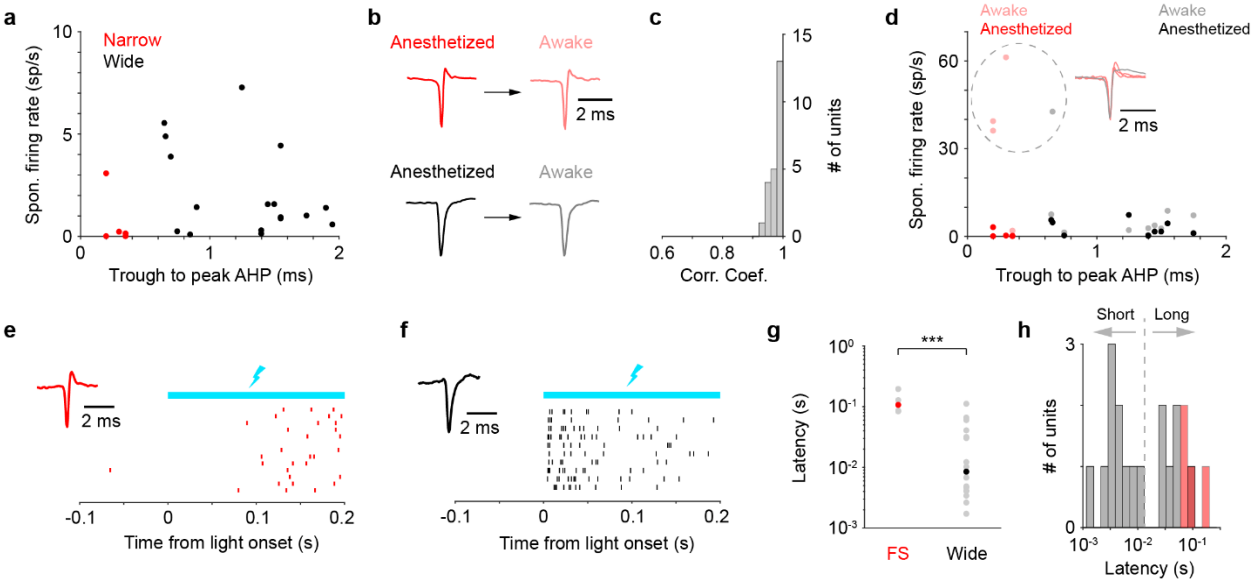

Figure 2. A subset of the units exhibited fast-spiking feature

(a) Scatter plot of spontaneous firing rate vs. trough to peak AHP for narrow (n = 5) and wide (n = 17) units under anesthesia.

(b) Example waveforms of the putative same units recorded in anesthetized (dark color) and awake state (light color).

(c) Histogram of spike waveform similarity (Pearson correlation coefficient) of the putative same units recorded in both states.

(d) Scatter plot of spontaneous firing rate vs. trough to peak AHP in anesthetized (dark color) and awake state (light color). A subset of units shown in (a) underwent both states (5 narrow and 9 wide units). 3 narrow units and 1 wide unit (circled) exhibited spontaneous firing rate > 30 spikes/s in the awake state, and were considered as fast-spiking. The waveforms of these units are shown next to the dashed circle.

(e) Example spike trains (ticks) to optogenetic stimulation of an FS unit, with 127 ms response latency to stimulation. Rows represent trials.

(f) Example spike trains (ticks) to optogenetic stimulation of a wide unit, with 5 ms response latency to stimulation. Rows represent trials.

(g) Comparison of response latency between FS (n = 4) and wide units (n = 16) during anesthesia with median indicated. FS vs. Wide, 106 (85, 160) ms vs. 8 (4, 36) ms, median (IQR), P = 1e-4.

(h) Histogram of response latency for FS and wide units shown in (g).

Therefore, reversed polarity units were excluded from the following analyses concerning spike width. We quantified the width of the typical spike waveforms based on trough to peak after-hyperpolarization (AHP) and full width at half maximum (FWHM, Fig. 1c). Trough to peak AHP was relatively widely distributed between 0.2 and 2 ms, while FWHM was more narrowly distributed and peaked around 0.2-0.3 ms (Fig. 1d). These results suggest that spike waveforms could be more separable using trough to peak AHP. Accordingly, we classified narrow and wide units based on a threshold between 0.4 and 0.6 ms trough to peak AHP (Totah et al., 2018), yielding 23% (5/22) narrow and 77% (17/22) wide units. The units appeared to form additional subclusters (Fig. 1e), which were further classified by K-means clustering (Methods), demonstrating that narrow units exclusively exhibited one waveform subclass which lacked the prolonged AHP, while wide units likely possessed different waveform subclasses (Fig. 1e, f).

The presence of narrow units in/around the mouse LC supports a recent rat study, where ~15% of the population (34/234) was found to be narrow (Totah et al., 2018). However, could the narrow units be fast-spiking interneurons (Breton-Provencher and Sur, 2019)? Under isoflurane anesthesia (2%), all units showed low spontaneous firing rate (0.6 (0.2, 1.7) spikes/s, median (IQR), Fig. 2a). A subset of the recordings was acquired in the awake state as well (<4 hours interval between anesthetized and awake states). In order to examine their awake firing rate, we first strove to ensure that the putatively same units were tracked in the two states by including the units that were acquired from the same tetrode channel in both states with highly similar waveforms (Fig. 2b, c. 5 narrow units, 9 wide units and 9 reversed polarity units. Waveform similarity, anesthesia vs. awake: 0.98 (0.96, 0.99), n = 23). In the awake state, we found that a fraction of these units exhibited >30 Hz spontaneous firing rate (Fig. 2d, circled ones). Together with their apparent narrow spike waveforms, these units were likely to be fast-spiking (FS) interneurons. Interestingly, all putative FS units had >80 ms response latency to tagging, longer than the classic wide units (FS vs. Wide, 106 (84, 160) vs. 8 (4, 36) ms, P = 1.0e-4, Fig. 2e-h), and longer than all non-FS units as well (FS vs. All, 106 (85, 160) ms vs. 12 (5, 38) ms, P = 0.0041). Our results suggest that a fraction of the narrow units in/around the LC are fast-spiking

143 interneurons. As a result, these FS units were excluded from further analysis, and the remaining
144 units were considered as LC NA+ neurons.
145

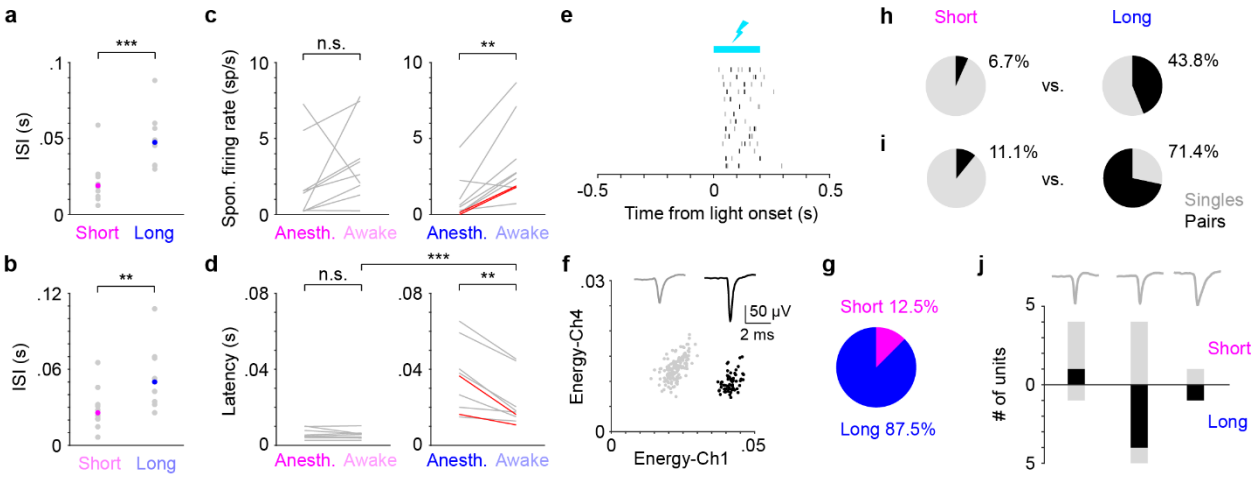

Figure 3. Different response properties of the units

(a) Comparison of ISI during anesthesia tagging between short and long latency units with median indicated. Short vs. Long, 19 (12, 21) ms vs. 47 (32, 57) ms, P = 9.7e-4. A total of 19 units underwent tagging in both anesthetized and awake states. Units with response latency < 12 ms were considered short latency (n = 10, magenta), > 12 ms considered long latency (n = 9, blue). Main results in Fig. 3 held when using 10 ms to classify latency. It is important to point out that in 2 recordings the evoked ISI is ≤10 ms. This does not translate to a sustained firing rate >100 spikes/s. Instead, it represents a short burst of spiking (typically 2 spikes) evoked by light.

(b) Comparison of ISI during awake tagging between short and long latency units with median indicated. Short vs. Long, 25 (21, 32) ms vs. 50 (34, 69) ms, P = 0.0082. Short and long latency units were classified in the anesthetized state.

(c) Comparisons of spontaneous firing rate between anesthetized and awake state for short and long latency units. Left: short latency units, 1.7 (0.2, 2.5) vs. 2.8 (2.0, 4.1) spikes/s, P = 0.13, n = 10; Right: long latency units, 0.4 (0.1, 0.8) vs. 2.8 (2.1, 4.6) spikes/s, P = 0.0039, n = 9. Two red lines indicate the two non-FS narrow units.

(d) Comparisons of response latency to tagging between anesthetized and awake state for short and long latency units. Left: short-latency units, 5 (4, 8) vs. 6 (4, 7) ms, P = 0.38, n = 10; Right: long-latency units, 36 (19, 45) vs. 17 (14, 26) ms, P = 0.0039, n = 9. Two red lines indicate the two non-FS narrow units. One long-latency narrow unit became short-latency under awake state.

(e) Example spike trains (ticks) to optogenetic stimulation of two distinct single units (grey and black) recorded from the same tetrode channel. We call these units 'pairs'.

(f) Spike sorting diagram and waveforms of the two units in (e). Units were identified in Ch1.

(g) Pie chart showing the percentage of short and long latency units in all unit pairs. Short vs. Long, 12.5% (1/8) vs. 87.5% (7/8), P = 0.0027, chi-squared test.

(h) Pie chart showing the percentage of unit pairs (black) in short and long latency unit groups during anesthesia. Short vs. Long, 6.7% (1/15) vs. 43.8% (7/16), P = 0.018, chi-squared test.

(i) Pie chart showing the percentage of unit pairs (black) in short and long latency wide unit groups during anesthesia. Short vs. Long, 11.1% (1/9) vs. 71.4% (5/7), P = 0.013, chi-squared test.

(j) Bar plot showing the number of singles (grey) and pairs (black) in the three subgroups of wide units (classified in Fig. 1e, f), separated by short and long latency. Same data as in (i). 2 unit pairs were of reserved polarity and not shown here.

LC neurons showed different response latencies to tagging (Fig. 2h). Since the latency distribution appeared to be bimodal separated around 10-12 ms, we considered < 12 ms as short latency, and > 12 ms as long latency (only two reversed polarity units had latency of 11 ms and would be classified differently). The identification of long latency units supports recent findings both *in vitro* and *in vivo* (Hickey et al., 2014; Li et al., 2016), suggesting heterogeneous excitability across LC neurons. Other lines of evidence further supported the possibility that the long latency units had lower excitability including: 1) the long latency units had longer ISI than the short latency units during tagging (Fig. 3a, b); and 2) transitioning from anesthetized to awake state only long latency units showed a significant increase of spontaneous firing rate, accompanied by a reduction of response latency (Fig. 3c, d). However, only one long latency unit (narrow) was turned to short latency in the awake state, and the latency difference between the two groups persisted (Short vs. Long in the awake state, P = 2.2e-5, with short and long latency defined in the anesthetized state, Fig. 3d), suggesting that behavioral states (anesthesia vs. awake) alone are insufficient to account for the differences in response latency.

As described previously, typically one tagged unit can be sorted from a recording, but a subset of recordings yielded multiple tagged units. Specifically, in a set of recordings two light-responsive single units were present in the same tetrode channel (Fig. 3e, f. We have never sorted more than two tagged units from one channel). A total of 8 such units were acquired from 4 recordings (6 wide units and 2 reversed polarity units), and we called them 'pairs'. Subsequently, the other units were called 'singles'. The fact that a single tetrode channel was able to pick up the spiking activity

of two distinct units suggests that the two units were spatially proximal to each other. Interestingly, among these 8 unit pairs, only 1 had a short response latency, and all the remaining units had long latencies (12.5% (1/8) vs. 87.5% (7/8), P = 0.0027, chi-squared test, Fig. 3g). We also found higher proportion of unit pairs in the long latency group compared with that in the short latency group when we included all units that were tested under anesthesia (6.7% (1/15) vs. 43.8% (7/16), P = 0.018, Fig. 3h), or all wide units tested under anesthesia (11.1% (1/9) vs. 71.4% (5/7), P = 0.013, Fig. 3i, j). Together, our data suggest a link between proximity and response latency, such that putatively proximal LC neurons tended to have a long response latency to optogenetic activation.

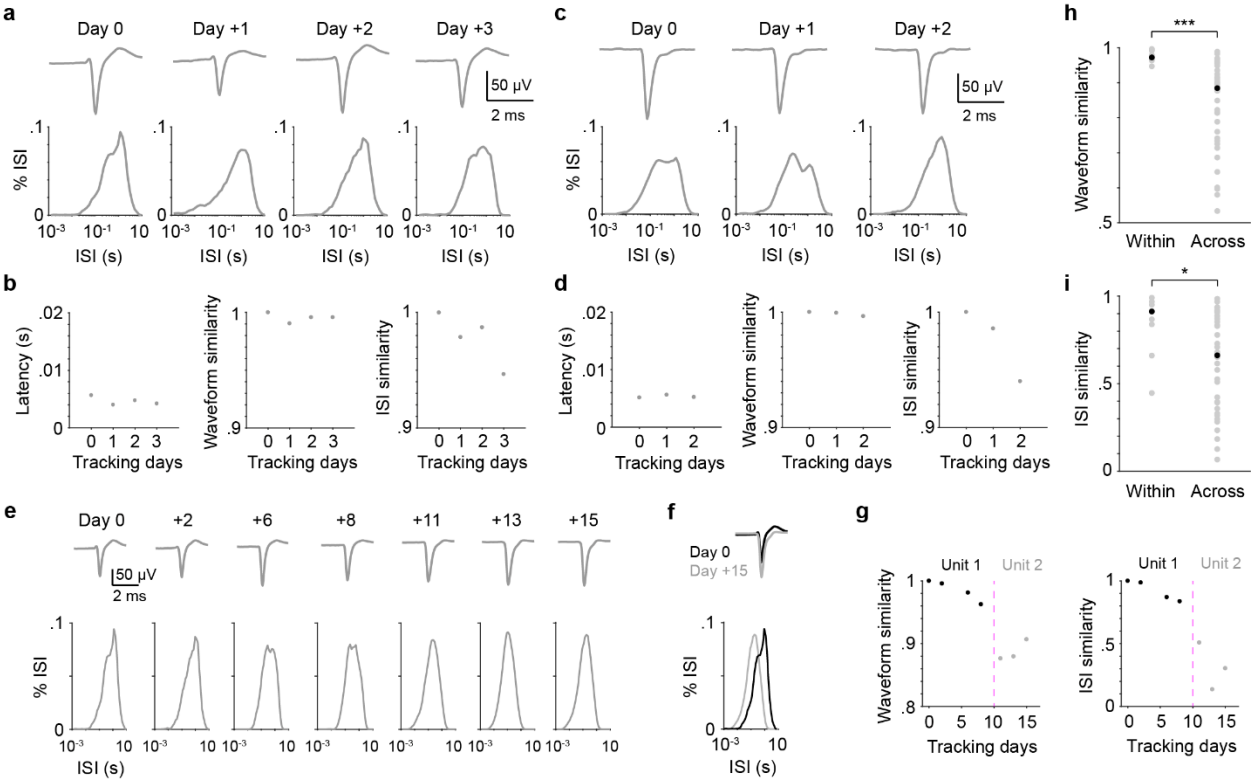

Figure 4. Tracking units across sessions

(a) Example spike waveforms and ISI distributions acquired from the same tetrode channel for 4 consecutive days during behavior.

(b) Response latency to tagging, spike waveform and ISI distribution similarities across the 4 days shown in (a). Similarity was quantified as the Pearson correlation coefficient between day 0 and each following day.

(c, d) Same conventions as in (a, b), but for recordings from a different mouse for 3 consecutive days.

(e) Same convention as in (a), but for recordings across 16 days.

(f) Overlay of spike waveforms and ISI distributions on the first day (day 0) and last day (day +15) shown in (e). Note that the AHP was prominent on day 0 but was much reduced on day +15.

(g) Same conventions as in (b) for the recordings in (e). Note the sharp decreases in both spike waveform and ISI similarities between day 8 and day 10 (magenta line), indicative of the transition from one unit to another.

(h) We used a spike waveform similarity threshold 0.95 to distinguish the putatively same units from the putatively distinct units, and obtained 9 putatively distinct units, each tracked for at least 2 sessions. Among these 9 units, spike waveforms from the putatively same units on the first day and last day (Within) were more similar than spike waveforms from the putatively different units on the first day (Across. Within vs. Across, Pearson correlation coefficient, 0.97 (0.97, 0.99) vs. 0.88 (0.73, 0.94), P = 6.7e-5). Gray dots: individual pairs. Black dots: group median.

(i) Same conventions as in (h), but for comparing ISI distribution within and across the 9 units. Within vs. Across, 0.91 (0.79, 0.95) vs. 0.66 (0.34, 0.88), P = 0.018.

Pupil diameter has been often treated as a noninvasive readout of LC activity (e.g., (Aston-Jones and Cohen, 2005; Gilzenrat et al., 2010; Preuschoff et al., 2011; Clewett et al., 2020)), but recent work challenged this view (Joshi et al., 2016; Yang et al., 2021; Megemont et al., 2022). We wondered whether physiological differences of LC neurons underlie their distinct relationship with pupil diameter. We further wondered whether the same neuron may correlate with pupil differently, i.e., exhibit session-to-session variability. If true, this would uncover another layer of variability and complexity when treating pupil diameter as a readout of LC activity. In this set of experiments, we recorded from single LC units with simultaneous pupil tracking in mice performing a tactile detection task (Methods). We acquired one session per day from each mouse for as long as a tagged unit was present. Therefore, testing these hypotheses requires to first distinguish the recordings of the putatively distinct LC units from the putatively identical units and then to examine their relationship with pupil diameter, respectively. To quantitatively assess whether the putatively same unit was tracked, we restricted analysis to a set of recordings with the following criterion: recordings across multiple days from the same mouse were included when in each recording the same tetrode channel contained a tagged unit. Across these multiple recordings from the same mouse, we compared spike waveform and ISI distribution on day 0 (first recording session) against spike waveform and ISI distribution on each following session/day (Methods). Both similarity measures stayed high across sessions, but ISI similarity appeared to have slightly bigger fluctuations (Fig. 4a-d). In few cases we observed more dramatic changes in both similarity

198 measures, suggesting a shift from recording one unit to another (Fig. 4e-g). Based on these
199 observations and a recent tracking study in the olfactory cortex (Schoonover et al., 2021), we
200 established a spike waveform similarity threshold of 0.95 to distinguish the putatively same units
201 from different units. Based on this metric, 9 putatively different units from 6 mice were tracked for
202 at least 2 sessions during behavior. This represents a low probability (<30%, 6 out of 21 mice) of
203 tracking LC neurons across days, demonstrating the challenges of this approach (Eschenko and
204 Sara, 2008). Spike waveform similarity from the putatively same unit across days (Within: day 0
205 vs. last day) was higher than the waveform similarity between the putatively different units (Across:
206 day 0, unit 1 vs. unit 2. Within vs. Across, 0.97 (0.97, 0.99) vs. 0.88 (0.73, 0.94), median (IQR), P
207 = 6.7e-5, Fig. 4h). In parallel, this metric was able to distinguish ISI similarity quantified within the
208 same unit from ISI similarity quantified across different units (Within vs. Across, 0.91 (0.79, 0.95)
209 vs. 0.66 (0.34, 0.88), P = 0.018, Fig. 4i).
210

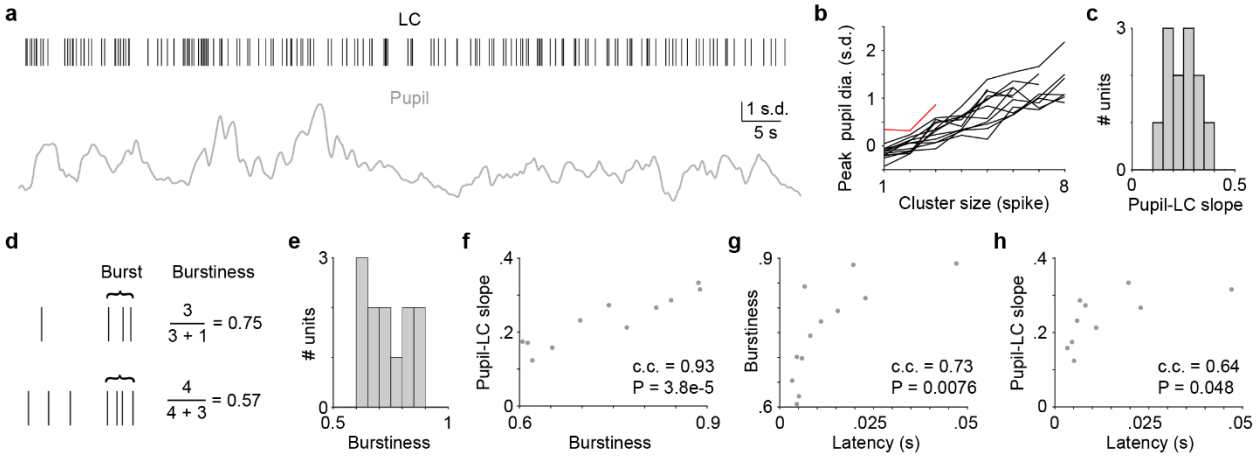

Figure 5. Pupil-LC relationship across distinct LC neurons

(a) Example simultaneously recorded LC spike train (ticks) and pupil diameter (z-scored).

(b) The relationship between peak pupil diameter and LC cluster size for all 13 distinct units. Relationships with linear regression $R^2 > 0.6$ in black (n = 12), < 0.6 in red (n = 1).

(c) Histogram of the pupil-LC slopes with $R^2 > 0.6$ in (b).

(d) Demonstration of the definition of burstiness.

(e) Histogram of burstiness for the 13 units in (b).

(f) The relationship between pupil-LC slopes and burstiness for the units with $R^2 > 0.6$ in (b). c.c.: Pearson correlation coefficient.

(g) The relationship between burstiness and response latency to tagging.

(h) The relationship between pupil-LC slopes and response latency to tagging.

211

With the ability to distinguish the recordings of the putatively distinct units from the putatively same units, we can now assess 1) whether LC physiological differences contribute to the variations in the pupil-LC relationship for distinct neurons, and 2) whether pupil-LC relationship exhibits session-to-session variations for the same neuron. To address the first question, we analyzed the relationship between pupil diameter and the putatively distinct LC units, using methods described in our recent study (Megemont et al., 2022). Briefly, we first grouped adjacent spikes into individual clusters based on each unit's ISI distribution and associated cluster size (number of spikes) to the amplitude of pupil dilation. Using a dataset that was largely different from our previous work (Methods), we recapitulated similar variations in the pupil-LC relationship (Fig. 5a-c). How we computed LC cluster reminisced the definition of burst firing in the literature (Fig. 5d, e, Methods, (Guido et al., 1992; Senzai et al., 2019)). However, these two measures can be dissociated from each other (see Discussion). With the attempt to further decorrelate the two measures, we used a fixed threshold of 0.1 s to define burst firing (burstiness). Consistent with the idea that pupil dilation better tracks phasic activity of LC neurons (e.g., (Aston-Jones and Cohen, 2005; Murphy et al., 2014; Reimer et al., 2016)), it is perhaps intuitive that the differences in burstiness of LC neurons correlated with the variations in the pupil-LC relationship, where more bursting neurons exhibited a stronger relationship with pupil dilation (Fig. 5f). Importantly, independent from clustering spikes, we found that response latency to tagging was positively correlated with both the degree of burstiness of LC neurons and their relationship with pupil diameter (Fig. 5g, h). Similar results held when we used a different method to define burstiness, or used other thresholds to quantify burst firing and pupil-LC relationship (Methods). Together, our data show that variations in response latency of LC neurons to optogenetic tagging was linked to their burst firing and distinct relationship with pupil diameter.

Next, we tested whether the pupil-LC relationship was variable for the same LC neuron across sessions. Examples from two distinct units showed noticeable session-to-session differences in their relationship with pupil, such that on different sessions identical amplitude of pupil dilation was linked to different LC activity (Fig. 6a, b). Overall, we were able to obtain the tracking of 4 distinct LC units across at least 3 sessions where monotonic pupil-LC relationships can be established (Methods). We compared the variation of pupil-LC slopes from each unit across sessions against the variation of pupil-LC slopes across distinct units (population). By resampling the population slopes to generate a reference distribution, we found that the variation of pupil-LC slopes within each individual unit was largely comparable to the population variation (Fig. 6c, d, Methods). Burstiness across sessions cannot account for the variation in the pupil-LC slopes

246 within individual units, while behavioral states (hit rate, false alarm rate) correlated with the pupil-
247 LC slopes in 2 out of the 4 units (Fig. 6e-g). These results demonstrate that session-to-session
248 fluctuations of the pupil-LC relationship for the putatively same unit are as variable as the neuron-
249 to-neuron fluctuations of this relationship. Together, our results uncovered a physiological
250 correlate of the pupil-LC relationship, and revealed two levels of variability in this relationship, i.e.,
251 across different neurons and within the same neuron.
252

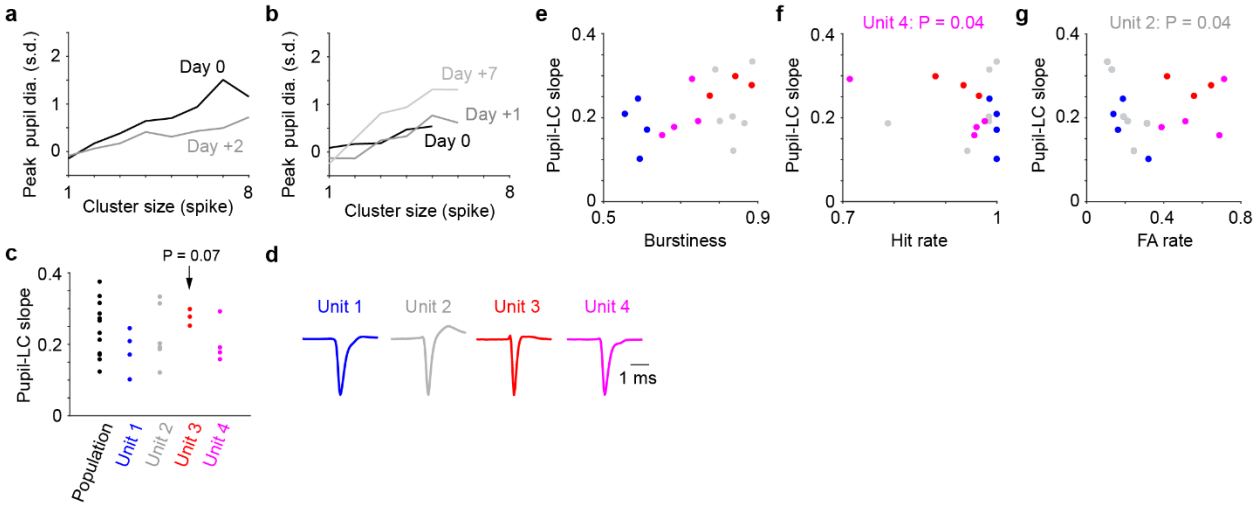

Figure 6. Pupil-LC relationship within the same LC neurons

(a-b) Example pupil-LC relationships for two distinct units tracked across days. (a): Pupil-LC slope on day 0: 0.21; day +2: 0.10. (b): Pupil-LC slope on day 0: 0.12; day +1: 0.19; day +7: 0.31.

(c) The variation of pupil-LC slopes within each individual unit was largely comparable to the variation of pupil-LC slopes across distinct units (population. Unit 1 vs. Population, P = 0.37; Unit 2 vs. Population, P = 0.29; Unit 3 vs. Population, P = 0.07; Unit 4 vs. Population, P = 0.32).

(d) Average waveforms of the 4 tracked units in (c).

(e) Scatter plot of pupil-LC slope vs. burstiness across sessions for individual units (same color code as in c, d). Unit 1: c.c. = -0.35, P = 0.65; Unit 2: c.c. = 0.08, P = 0.88; Unit 3: c.c. = 0.65, P = 0.56; Unit 4: c.c. = 0.61, P = 0.39.

(f) Scatter plot of pupil-LC slope vs. Hit rate across sessions for individual units. Unit 1: c.c. = -0.69, P = 0.31; Unit 2: c.c. = 0.41, P = 0.42; Unit 3: c.c. = -0.97, P = 0.14; Unit 4: c.c. = -0.95, P = 0.04.

(g) Scatter plot of pupil-LC slope vs. False alarm rate across sessions for individual units. Unit 1: c.c. = -0.78, P = 0.29; Unit 2: c.c. = -0.82, P = 0.04; Unit 3: c.c. = -0.57, P = 0.63; Unit 4: c.c. = 0.46, P = 0.54. c.c., Pearson correlation coefficient.

253

Discussion

We provide a unique dataset to explore heterogeneity in the mouse LC. Our sample size may appear small compared to other studies that recorded from non-opto-tagged units. However, to our knowledge, the current study presents one of the largest *in vivo* datasets of opto-tagged units in the LC to study its physiological and functional heterogeneity.

Our data showed that a fraction, but not all of the narrow units in the LC were fast spiking. A recent study reported the existence of ~15% narrow units in rats (Totah et al., 2018), where LC neurons were identified under anesthesia by 'pharmacological tagging', i.e., their spiking activity can be silenced by α2 receptor agonist. However, a mouse study implied that the narrow units could be GABAergic interneurons (Breton-Provencher and Sur, 2019). Based on our data, it is possible that the non-FS narrow units are NA+ (~10%, 2/18). At the same time, our data suggest that a sizable proportion of the narrow units identified under anesthesia are fast-spiking interneurons, as anesthesia could inhibit and suppress their fast-spiking feature (Patel et al., 1999; Zhao et al., 2021).

Intracellular studies have reported AHP amplitude differences on the order of several millivolts among different LC populations (e.g., (Chandler et al., 2014; Wagner-Altendorf et al., 2019)). This may account for the different spike waveforms within the wide units, but it is unlikely to explain the absence of the extracellularly measured slow AHP component in the narrow units. We speculate that the narrow units may have lower expression of the small-conductance, Ca^{2+}-activated K^+ (SK) channels, which are known to mediate the prolonged AHP in neurons including the LC (Louise Faber and Sah, 2003; Adelman et al., 2012; Matschke et al., 2018). We did not have access to identifying the location of the recorded units, but in rats narrow units were found to be distributed toward the ventral LC (Totah et al., 2018), which may preferentially innervate the spinal cord (Li et al., 2016; Hirschberg et al., 2017).

We found a considerable proportion of putative LC NA+ neurons with long response latency to optogenetic activation despite of anesthetized or awake state (~40%, 8/19). We drove the expression of ChR2 monoallelically by crossing two mouse lines (*DBH-Cre;Ai32*). Thus, response latency differences should not be due to variations in ChR2 expression across DBH+ neurons. Although we cannot rule out the possibility that long response latency on the order of several tens of milliseconds could be a result of indirect activation (McCall et al., 2015), it has been reported

that a sizable fraction (~30%, 2/6) of ChR2-expressing LC NA+ neurons *in vitro* can only be activated to emit spikes with prolonged illumination (> 100 ms, (Hickey et al., 2014)). An *in vivo* study also identified a fraction (~40%) of LC neurons that can only be excited by long pulses (4/9 neurons required >200 ms pulses, (Li et al., 2016)). These lines of evidence lead to the possibility of heterogeneous excitability among LC neurons. Since NA inhibits LC activity (Cedarbaum and Aghajanian, 1976; Aghajanian et al., 1977; Egan et al., 1983; Foote et al., 1983), it is plausible that the long latency units are inhibited by nearby opto-activated LC neurons. Specifically, a recent modeling study predicts that spatially adjacent LC neurons can mutually inhibit each other via NA acting on α2 receptors (Baral et al., 2022). We noticed that if two LC units were recorded by one tetrode channel (unit pairs), these units were more likely to have a long response latency. Our tetrode wires have nominal impedance of 200-500kΩ, thus should be sensitive to spiking signal within ~100 μm radius (c.f. (Barthó et al., 2004; Jun et al., 2017)). The discovery of long latency unit pairs supports this prediction (Baral et al., 2022), suggesting that long response latency to optogenetic activation reflects enhanced mutual inhibition and reduced excitability in a set of LC neurons. If true, the activity of these neurons would be more likely to be anticorrelated. However, our data are insufficient to test such hypothesis (3 out of 8 unit pairs were confirmed to underwent tagging in the awake state, and none was recorded during behavior). Future studies (both *in vitro* and *in vivo*) are needed to test these conjectures.

Although both LC cluster and burstiness were defined in similar ways, burstiness took longer baseline activity into account for normalization. As a result, a given cluster size could correspond to different levels of burstiness. On the other hand, response latency to tagging was completely independent from the methodology of clustering LC spikes but was found to be correlated with burstiness and pupil-LC relationship. Therefore, our results suggest that the excitability of LC neurons underlies their firing patterns and the relationship with pupil diameter.

We revealed two levels of variability in the pupil-LC relationship, i.e., across different neurons and within the same neuron, substantiating and extending previous conclusions that pupil diameter is not an accurate readout of LC activity. What underlies the session-to-session fluctuations of the pupil-LC relationship within individual LC neurons? Technical limitations in the current study may have restricted the statistical power to fully address this important question, as it is rare that the putatively same neuron can be recorded over multiple days for reliably assessing its relationship with pupil. However, based on the literature, we speculate that the pupil-LC relationship is modulated by various external and internal factors, including LC physiological heterogeneity,

behavioral states and input from other brain regions (Joshi et al., 2016; Cazettes et al., 2020; Megemont et al., 2022). Importantly, these factors may not be completely independent from one another, e.g., behavioral states may influence burst firing, and different behavioral states could engage different neural circuits.

Author contributions

LST, JML and HY planned the project. LST and JML performed experiments. LST, JML and HY analyzed data with assistance from MG, MM and MR. MM, MG and HY wrote the manuscript with contributions from all authors. HY supervised research.

Acknowledgements

We thank Viji Santhakumar, Deepak Subramanian, Edward Zagha and Sachiko Haga-Yamanaka for comments on the manuscript. MR was supported by NIH grants (R01NS104026, R21MH118640). HY was supported by UCR startup, Klingenstein-Simons Fellowship Awards in Neuroscience, and NIH grants (R01NS107355, R01NS112200).

Data availability. Data are available from the corresponding author upon request.

Code availability. MATLAB scripts used to analyze the data are available from the corresponding author upon request.

Competing interest. The authors declare no potential conflict of interest.

Materials and Methods

All procedures were performed in accordance with protocols approved by UC Riverside Animal Care and Use Committee (AUP 20190031). Mice were DBH-Cre (B6.FVB(Cg)-Tg(Dbh-cre) KH212Gsat/Mmucd, 036778-UCD, MMRRC); Ai32 (RCL-ChR2(H134R)/EYFP, 024109, JAX), singly housed in a vivarium with reverse light-dark cycle (9a-9p). Male and female mice of 8-12 weeks were implanted with titanium head posts as described previously (Yang et al., 2016). Procedures for microdrive construction and LC recording have been described previously (Yang et al., 2021; Megemont et al., 2022). Briefly, custom microdrives with eight tetrodes and an optic fiber (0.39 NA, 200 um core) were built and implanted in the left LC to make extracellular recordings. At the conclusion of the experiments, brains were perfused with PBS followed by 4% PFA, post-fixed overnight, then cut into 100 µm coronal sections and stained with anti-Tyrosine Hydroxylase (TH) antibody (Thermo-Fisher OPA1-04050).

Behavior task was controlled by BControl (C. Brody, Princeton University) or custom-based Arduino hardware and software as described previously (Yang et al., 2016, 2021; McBurney-Lin et al., 2020). Video of the left pupil (ipsilateral to LC recording and stimulation) was acquired at 50 Hz using a PhotonFocus camera and StreamPix 5 software, or at 20 Hz using a Basler acA1300-200um camera and Pylon software. 450 nM blue diode lasers (UltraLasers, MDL-III-450-200mW) controlled by WaveSurfer (https://www.janelia.org/open-science/wavesurfer) were used for optogenetic stimulation. Pupil diameter was extracted using DeepLabCut (Mathis et al., 2018). Electrophysiology and pupil tracking were synchronized via a common TTL pulse train. The mating sleeve connecting two ferrules was covered with black tape to prevent light leak. An ambient blue LED was used to constrict the pupil and to mask any potential light leak. Optogenetic stimulation for tagging consisted of a train of 200 or 300-ms pulses delivered at 0.3-0.5 Hz and 10 mW (RMS, measured at the tip of optical fiber). Tagging was performed during anesthesia (2% isoflurane) and sometimes during awake, non-task performing condition. Mice were trained to perform a go/no-go single-whisker detection task as described previously (McBurney-Lin et al., 2020; Yang et al., 2021) or a variant of this task. Briefly, in the original task, licking to the deflection of the right C2 whisker (go trials) resulted in a water reward (Hit). Licking in the absence of whisker deflection (no-go trials) resulted in a timeout (False alarm). The main difference in the variant task is that on no-go trials, the contralateral whisker (left C2) was deflected, instead of no whisker deflection (similar to (Aruljothi et al., 2020)). All trial type classifications followed the original task.

Spike sorting was performed using MClust (Redish, 2014). 35 distinct single units (clustering quality measure, L_{ratio}: 0.005 ± 0.002) from 26 recordings of 21 mice were included. 13 units with reversed polarity were excluded from the analyses concerning spike width. K-means clustering used trough to peak AHP and FWHM to classify waveforms in Fig. 1e, f. Spike waveform similarity was defined as the Pearson correlation coefficient between two waveforms (± 2 ms from trough). ISI distribution was generated by logarithmic binning between 0.001 and 10 s. ISI distribution similarity was defined as the Pearson correlation coefficient between two distributions. Spontaneous firing rate in Fig. 2 and 3 were extracted from the tagging sessions as well, quantified as the average firing rate in a 1-s window before the onset of each stimulation pulse. For Fig. 4, 9 putatively different units from 6 mice were tracked for at least 2 sessions during behavior. Results in Fig. 4i held when using a spike waveform similarity threshold between 0.93 and 0.96 to distinguish the putatively same units from different units. For Fig. 5b, 13 distinct units from 13 recordings of 9 mice were included. 5 recordings were with the original task (Megemont et al., 2022) and 8 recordings were with the variant task. To quantify the pupil-LC relationship, adjacent LC spikes were grouped into individual clusters based on each unit's median inter-spike interval (Megemont et al., 2022). Pupil response associated with each spike cluster was quantified as the maximum pupil diameter in a 6-s window following the onset of the cluster (time of the first spike). 12 recordings were with linear regression of pupil-LC relationship R^2>0.6 (black curves in Fig. 5b). Outlier test removed one recording from the analysis of pupil-LC slopes vs. burstiness in Fig. 5f.

LC burst was defined the same way as spike cluster but with a fixed threshold of 0.1 s to group spikes. The burstiness of each burst was quantified as the number of spikes in the burst divided by the total number of spikes in a time window starting 0.5-s prior to the burst onset and ending at the end of the burst. Results in Fig. 5f-h were robust when LC cluster or burstiness was defined with other variable or fixed thresholds. For example, when the threshold for cluster was 0.2 s and the threshold for burstiness was 25% ISI, statistics in Fig. 5f-h would become c.c. = 0.89, P = 5.6e-4; c.c. = 0.63, P = 0.039; c.c. = 0.73, P = 0.025, respectively. We further tested the robustness of these results by defining burstiness in a different way, following a recent work (Senzai et al., 2019). Specifically, burstiness was quantified as the ratio of the number of spikes in 1 ms – 20% ISI bins (we have tested between 10% and 30%) of the spike autocorrelogram and the number of spikes in 500 – 1000 ms bins, and the threshold for LC cluster was 0.2 s. Statistics in Fig. 5f-h would become c.c. = 0.88, P = 6.9e-4; c.c. = 0.70, P = 0.016; c.c. = 0.73, P = 0.025, respectively.

Out of the 9 tracked units in Fig. 4, 4 units were tracked for at least 3 sessions with pupil-LC relationship R^2>0.6, and were included in Fig. 6c-g. To compare the variation of pupil-LC slopes across distinct LC units (population) with the variation of the same unit across sessions, population slopes were redrawn 1000 times to generate a null distribution of variance, and each time the number of samples drawn matched the number of sessions from each unit. The reported P values in Fig. 6c represented the proportion of iterations where the population variance across distinct units was smaller than the across-session variance within individual units.

Data were reported as median (interquartile range, IQR) unless otherwise noted. We did not use statistical methods to predetermine sample sizes. Sample sizes are similar to those reported in the field. We assigned mice to experimental groups arbitrarily, without randomization or blinding. When sample size was >7, we used two-tailed sign rank test for paired comparisons and two-tailed rank sum test for unpaired comparisons. When sample size was ≤ 7, we used two-tailed paired or unpaired t-test, respectively, unless otherwise noted.

References

Adelman JP, Maylie J, Sah P (2012) Small-conductance Ca 2+-activated K + channels: Form and function. Annu Rev Physiol 74:245–269.

Aghajanian GK, Cedarbaum JM, Wang RY (1977) Evidence for norepinephrine-mediated collateral inhibition of locus coeruleus neurons. Brain Res 136:570–577.

Andrade R, Aghajanian GK (1984) Locus coeruleus activity in vitro: intrinsic regulation by a calcium-dependent potassium conductance but not alpha 2-adrenoceptors. J Neurosci 4:161–170.

Aruljothi K, Marrero K, Zhang Z, Zareian B, Zagha E (2020) Functional Localization of an Attenuating Filter within Cortex for a Selective Detection Task in Mice. J Neurosci 40:JN-RM-2993-19.

Aston-Jones G, Bloom FE (1981) Activity of norepinephrine-containing locus coeruleus neurons in behaving rats anticipates fluctuations in the sleep-waking cycle. J Neurosci 1:876–886 Available at: http://www.ncbi.nlm.nih.gov/pubmed/7346592.

Aston-Jones G, Cohen JD (2005) An integrative theory of locus coeruleus-norepinephrine function: Adaptive gain and optimal performance. Annu Rev Neurosci 28:403–450.

Baral S, Hosseini H, More K, Fabrin TMC, Braun J, Prigge M (2022) Spike-Dependent Dynamic Partitioning of the Locus Coeruleus Network through Noradrenergic Volume Release in a Simulation of Nucleus Core. Brain Sci 12:728 Available at: https://www.mdpi.com/2076-3425/12/6/728.

Barry JM (2015) Axonal Activity in vivo: Technical considerations and implications for the exploration of neural circuits in freely moving animals. Front Neurosci 9:1–12.

Barthó P, Hirase H, Monconduit L, Zugaro M, Harris KD, Buzsáki G (2004) Characterization of neocortical principal cells and interneurons by network interactions and extracellular features. J Neurophysiol 92:600–608.

Berridge CW, Waterhouse BD (2003) The locus coeruleus-noradrenergic system: Modulation of behavioral state and state-dependent cognitive processes. Brain Res Rev 42:33–84 Available at: http://www.ncbi.nlm.nih.gov/pubmed/12668290.

Borodovitsyna O, Duffy BC, Pickering AE, Chandler DJ (2020) Anatomically and functionally distinct locus coeruleus efferents mediate opposing effects on anxiety-like behavior. Neurobiol Stress 13:100284 Available at: https://doi.org/10.1016/j.ynstr.2020.100284.

Breen LA, Burde RM, Loewy AD (1983) Brainstem connections to the Edinger-Westphal nucleus of the cat: a retrograde tracer study. Brain Res 261:303–306.

492 Breton-Provencher V, Sur M (2019) Active control of arousal by a locus coeruleus GABAergic
493 circuit. Nat Neurosci 22:218–228 Available at:
494 https://www.biorxiv.org/content/early/2018/09/09/412338.
495 Cazettes F, Reato D, Morais JP, Renart A, Mainen ZF (2020) Phasic Activation of Dorsal Raphe
496 Serotonergic Neurons Increases Pupil Size. Curr Biol:1–6.
497 Cedarbaum JM, Aghajanian GK (1976) Noradrenergic neurons of the locus coeruleus: inhibition
498 by epinephrine and activation by the α-antagonist piperoxane. Brain Res 112:413–419.
499 Chandler DJ, Gao W-J, Waterhouse BD (2014) Heterogeneous organization of the locus
500 coeruleus projections to prefrontal and motor cortices. Proc Natl Acad Sci U S A 111:6816–
501 6821.
502 Chandler DJ, Jensen P, McCall JG, Pickering AE, Schwarz LA, Totah NK (2019) Redefining
503 Noradrenergic Neuromodulation of Behavior: Impacts of a Modular Locus Coeruleus
504 Architecture. J Neurosci 39:8239–8249.
505 Clewett D, Gasser C, Davachi L (2020) Pupil-linked arousal signals track the temporal
506 organization of events in memory. Nat Commun 11:1–14 Available at:
507 http://dx.doi.org/10.1038/s41467-020-17851-9.
508 Egan TM, Henderson G, North RA, Williams JT (1983) Noradrenaline-mediated synaptic
509 inhibition in rat locus coeruleus neurones. J Physiol 345:477–488.
510 Eschenko O, Sara SJ (2008) Learning-dependent, transient increase of activity in noradrenergic
511 neurons of locus coeruleus during slow wave sleep in the rat: Brain stem-cortex interplay
512 for memory consolidation? Cereb Cortex 18:2596–2603.
513 Fallon JH, Loughlin SE (1982) Monoamine innervation of the forebrain: Collateralization. Brain
514 Res Bull 9:295–307.
515 Foote SL, Bloom FE, Aston-Jones G (1983) Nucleus locus ceruleus: new evidence of
516 anatomical and physiological specificity. Physiol Rev 63:844–914 Available at:
517 http://www.physiology.org/doi/10.1152/physrev.1983.63.3.844.
518 Gilzenrat MS, Nieuwenhuis S, Jepma M, Cohen JD (2010) Pupil diameter tracks changes in
519 control state predicted by the adaptive gain theory of locus coeruleus function. Cogn Affect
520 Behav Neurosci 10:252–269 Available at:
521 http://www.pubmedcentral.nih.gov/articlerender.fcgi?artid=3403821&tool=pmcentrez&rend
522 ertype=abstract [Accessed July 9, 2014].
523 Gold C, Henze DA, Koch C, Buzsáki G (2006) On the origin of the extracellular action potential
524 waveform: A modeling study. J Neurophysiol 95:3113–3128.
525 Guido W, Lu SM, Sherman SM (1992) Relative contributions of burst and tonic responses to the

receptive field properties of lateral geniculate neurons in the cat. J Neurophysiol 68:2199–2211.

Hickey L, Li Y, Fyson SJ, Watson TC, Perrins R, Hewinson J, Teschemacher a. G, Furue H, Lumb BM, Pickering a. E (2014) Optoactivation of Locus Ceruleus Neurons Evokes Bidirectional Changes in Thermal Nociception in Rats. J Neurosci 34:4148–4160 Available at: http://www.jneurosci.org/cgi/doi/10.1523/JNEUROSCI.4835-13.2014.

Hirschberg S, Li Y, Randall A, Kremer EJ, Pickering AE (2017) Functional dichotomy in spinal- vs prefrontal-projecting locus coeruleus modules splits descending noradrenergic analgesia from ascending aversion and anxiety in rats. Elife 6:1–26.

Joshi S, Li Y, Kalwani RM, Gold JI (2016) Relationships between Pupil Diameter and Neuronal Activity in the Locus Coeruleus, Colliculi, and Cingulate Cortex. Neuron 89:221–234 Available at: http://dx.doi.org/10.1016/j.neuron.2015.11.028.

Jun JJ et al. (2017) Fully integrated silicon probes for high-density recording of neural activity. Nature 551:232–236 Available at: http://dx.doi.org/10.1038/nature24636.

Kebschull JM, Garcia da Silva P, Reid AP, Peikon ID, Albeanu DF, Zador AM (2016) High-Throughput Mapping of Single-Neuron Projections by Sequencing of Barcoded RNA. Neuron 91:975–987 Available at: http://dx.doi.org/10.1016/j.neuron.2016.07.036.

Kempadoo KA, Mosharov E V., Choi SJ, Sulzer D, Kandel ER (2016) Dopamine release from the locus coeruleus to the dorsal hippocampus promotes spatial learning and memory. Proc Natl Acad Sci 113:14835–14840 Available at: http://www.pnas.org/lookup/doi/10.1073/pnas.1616515114.

Li Y, Hickey L, Perrins R, Werlen E, Patel AA, Hirschberg S, Jones MW, Salinas S, Kremer EJ, Pickering AE (2016) Retrograde optogenetic characterization of the pontospinal module of the locus coeruleus with a canine adenoviral vector. Brain Res 1641:274–290 Available at: http://dx.doi.org/10.1016/j.brainres.2016.02.023.

Liu Y, Rodenkirch C, Moskowitz N, Schriver B, Wang Q (2017) Dynamic Lateralization of Pupil Dilation Evoked by Locus Coeruleus Activation Results from Sympathetic, Not Parasympathetic, Contributions. Cell Rep 20:3099–3112 Available at: https://doi.org/10.1016/j.celrep.2017.08.094.

Loughlin SE, Foote SL, Fallon JH (1982) Locus coeruleus projections to cortex: Topography, morphology and collateralization. Brain Res Bull 9:287–294.

Louise Faber ES, Sah P (2003) Calcium-activated potassium channels: Multiple contributions to neuronal function. Neuroscientist 9:181–194.

Macosko EZ, Basu A, Satija R, Nemesh J, Shekhar K, Goldman M, Tirosh I, Bialas AR,

560 Kamitaki N, Martersteck EM, Trombetta JJ, Weitz DA, Sanes JR, Shalek AK, Regev A,
561 McCarroll SA (2015) Highly parallel genome-wide expression profiling of individual cells
562 using nanoliter droplets. Cell 161:1202–1214 Available at:
563 http://dx.doi.org/10.1016/j.cell.2015.05.002.
564 Mathis A, Mamidanna P, Cury KM, Abe T, Murthy VN, Mathis MW, Bethge M (2018)
565 DeepLabCut: markerless pose estimation of user-defined body parts with deep learning.
566 Nat Neurosci 21:1281–1289 Available at: http://dx.doi.org/10.1038/s41593-018-0209-y.
567 Matschke LA, Rinné S, Snutch TP, Oertel WH, Dolga AM, Decher N (2018) Calcium-activated
568 SK potassium channels are key modulators of the pacemaker frequency in locus coeruleus
569 neurons. Mol Cell Neurosci 88:330–341 Available at:
570 https://doi.org/10.1016/j.mcn.2018.03.002.
571 McBurney-Lin J, Lu J, Zuo Y, Yang H (2019) Locus coeruleus-norepinephrine modulation of
572 sensory processing and perception: A focused review. Neurosci Biobehav Rev 105.
573 McBurney-Lin J, Sun Y, Tortorelli LS, Nguyen QAT, Haga-Yamanaka S, Yang H (2020)
574 Bidirectional pharmacological perturbations of the noradrenergic system differentially affect
575 tactile detection. Neuropharmacology 174.
576 McCall JG, Al-Hasani R, Siuda ER, Hong DY, Norris AJ, Ford CP, Bruchas MR (2015) CRH
577 Engagement of the Locus Coeruleus Noradrenergic System Mediates Stress-Induced
578 Anxiety. Neuron 87:605–620 Available at: http://dx.doi.org/10.1016/j.neuron.2015.07.002.
579 Megemont M, McBurney-Lin J, Yang H (2022) Pupil diameter is not an accurate real-time
580 readout of locus coeruleus activity. Elife 11:1–17 Available at:
581 https://elifesciences.org/articles/70510.
582 Mulvey B, Bhatti DL, Gyawali S, Lake AM, Kriaucionis S, Ford CP, Bruchas MR, Heintz N,
583 Dougherty JD (2018) Molecular and Functional Sex Differences of Noradrenergic Neurons
584 in the Mouse Locus Coeruleus. Cell Rep 23:2225–2235.
585 Murphy PR, O'Connell RG, O'Sullivan M, Robertson IH, Balsters JH (2014) Pupil diameter
586 covaries with BOLD activity in human locus coeruleus. Hum Brain Mapp 35:4140–4154.
587 Patel AJ, Honoré E, Lesage F, Fink M, Romey G, Lazdunski M (1999) Inhalational anesthetics
588 activate two-pore-domain background K+ channels. Nat Neurosci 2:422–426.
589 Plummer NW, Scappini EL, Smith KG, Tucker CJ, Jensen P (2017) Two Subpopulations of
590 Noradrenergic Neurons in the Locus Coeruleus Complex Distinguished by Expression of
591 the Dorsal Neural Tube Marker Pax7. Front Neuroanat 11:1–11 Available at:
592 http://journal.frontiersin.org/article/10.3389/fnana.2017.00060/full.
593 Poe GR, Foote S, Eschenko O, Johansen JP, Bouret S, Aston-Jones G, Harley CW, Manahan-

Vaughan D, Weinshenker D, Valentino R, Berridge C, Chandler DJ, Waterhouse B, Sara SJ (2020) Locus coeruleus: a new look at the blue spot. Nat Rev Neurosci Available at: http://dx.doi.org/10.1038/s41583-020-0360-9.

Preuschoff K, 't Hart BM, Einhäuser W (2011) Pupil dilation signals surprise: Evidence for noradrenaline's role in decision making. Front Neurosci 5:1–12.

Privitera M, Ferrari KD, von Ziegler LM, Sturman O, Duss SN, Floriou-Servou A, Germain P, Vermeiren Y, Wyss MT, De Deyn PP, Weber B, Bohacek J (2020) A complete pupillometry toolbox for real-time monitoring of locus coeruleus activity in rodents. Nat Protoc Available at: http://dx.doi.org/10.1038/s41596-020-0324-6.

Rajkowski J, Kubiak P, Aston-Jones G (1994) Locus coeruleus activity in monkey: Phasic and tonic changes are associated with altered vigilance. Brain Res Bull 35:607–616.

Rall W, Shepherd GM (1968) Theoretical reconstruction of field potentials and dendrodendritic synaptic interactions in olfactory bulb. J Neurophysiol 31:884–915.

Redish AD (2014) MClust Spike sorting toolbox Documentation for version 4.4. Available at: http://redishlab.neuroscience.umn.edu/MClust/MClust-4.4.pdf.

Reimer J, McGinley MJ, Liu Y, Rodenkirch C, Wang Q, McCormick DA, Tolias AS (2016) Pupil fluctuations track rapid changes in adrenergic and cholinergic activity in cortex. Nat Commun 7:1–7 Available at: http://dx.doi.org/10.1038/ncomms13289.

Robertson SD, Plummer NW, de Marchena J, Jensen P (2013) Developmental origins of central norepinephrine neuron diversity. Nat Neurosci 16:1016–1023 Available at: http://www.ncbi.nlm.nih.gov/pubmed/23852112.

Sara SJ, Bouret S (2012) Orienting and Reorienting: The Locus Coeruleus Mediates Cognition through Arousal. Neuron 76:130–141 Available at: http://dx.doi.org/10.1016/j.neuron.2012.09.011.

Schoonover CE, Ohashi SN, Axel R, Fink AJP (2021) Representational drift in primary olfactory cortex. Nature 594:541–546 Available at: http://dx.doi.org/10.1038/s41586-021-03628-7.

Schwarz LA, Miyamichi K, Gao XJ, Beier KT, Weissbourd B, DeLoach KE, Ren J, Ibanes S, Malenka RC, Kremer EJ, Luo L (2015) Viral-genetic tracing of the input–output organization of a central noradrenaline circuit. Nature 524:88–92 Available at: http://www.nature.com/doifinder/10.1038/nature14600.

Senzai Y, Fernandez-Ruiz A, Buzsáki G (2019) Layer-Specific Physiological Features and Interlaminar Interactions in the Primary Visual Cortex of the Mouse. Neuron 101:500-513.e5.

Shekhar K, Lapan SW, Whitney IE, Tran NM, Macosko EZ, Kowalczyk M, Adiconis X, Levin JZ,

628 Nemesh J, Goldman M, McCarroll SA, Cepko CL, Regev A, Sanes JR (2016)
629 Comprehensive Classification of Retinal Bipolar Neurons by Single-Cell Transcriptomics.
630 Cell 166:1308-1323.e30 Available at: http://dx.doi.org/10.1016/j.cell.2016.07.054.
631 Sun SH, Almasi A, Yunzab M, Zehra S, Hicks DG, Kameneva T, Ibbotson MR, Meffin H (2021)
632 Analysis of extracellular spike waveforms and associated receptive fields of neurons in cat
633 primary visual cortex. J Physiol 599:2211–2238 Available at:
634 https://onlinelibrary.wiley.com/doi/10.1113/JP280844.
635 Tervo DGR, Hwang BY, Viswanathan S, Gaj T, Lavzin M, Ritola KD, Lindo S, Michael S,
636 Kuleshova E, Ojala D, Huang CC, Gerfen CR, Schiller J, Dudman JT, Hantman AW,
637 Looger LL, Schaffer D V., Karpova AY (2016) A Designer AAV Variant Permits Efficient
638 Retrograde Access to Projection Neurons. Neuron 92:372–382 Available at:
639 http://dx.doi.org/10.1016/j.neuron.2016.09.021.
640 Totah NK, Neves RM, Panzeri S, Logothetis NK, Eschenko O (2018) The Locus Coeruleus Is a
641 Complex and Differentiated Neuromodulatory System. Neuron 99:1055-1068.e6 Available
642 at: https://linkinghub.elsevier.com/retrieve/pii/S0896627318306354.
643 Uematsu A, Tan BZ, Ycu EA, Cuevas JS, Koivumaa J, Junyent F, Kremer EJ, Witten IB,
644 Deisseroth K, Johansen JP (2017) Modular organization of the brainstem noradrenaline
645 system coordinates opposing learning states. Nat Neurosci 20:1602–1611 Available at:
646 http://www.nature.com/doifinder/10.1038/nn.4642.
647 Varazzani C, San-Galli a., Gilardeau S, Bouret S (2015) Noradrenaline and Dopamine Neurons
648 in the Reward/Effort Trade-Off: A Direct Electrophysiological Comparison in Behaving
649 Monkeys. J Neurosci 35:7866–7877 Available at:
650 http://www.jneurosci.org/cgi/doi/10.1523/JNEUROSCI.0454-15.2015.
651 Wagner-Altendorf TA, Fischer B, Roeper J (2019) Axonal projection-specific differences in
652 somatodendritic α2 autoreceptor function in locus coeruleus neurons. Eur J Neurosci
653 50:3772–3785.
654 Waterhouse BD, Border B, Wahl L, Mihailoff GA (1993) Topographic organization of rat locus
655 coeruleus and dorsal raphe nuclei: Distribution of cells projecting to visual system
656 structures. J Comp Neurol 336:345–361.
657 Yang H, Bari BA, Cohen JY, O'Connor DH (2021) Locus coeruleus spiking differently correlates
658 with S1 cortex activity and pupil diameter in a tactile detection task. Elife 10:1–14 Available
659 at: https://elifesciences.org/articles/64327.
660 Yang H, Kwon SE, Severson KS, O'Connor DH (2016) Origins of choice-related activity in
661 mouse somatosensory cortex. Nat Neurosci 19:127–134 Available at:

http://www.nature.com/doifinder/10.1038/nn.4183.

Zhao W, Zhao S, Zhu T, Ou M, Zhang D, Sun H, Liu J, Chen X, Hemmings HC, Zhou C (2021) Isoflurane Suppresses Hippocampal High-frequency Ripples by Differentially Modulating Pyramidal Neurons and Interneurons in Mice. Anesthesiology:122–135.

Zingg B, Peng B, Huang J, Tao HW, Zhang LI (2020) Synaptic Specificity and Application of Anterograde Trans-Synaptic AAV for Probing Neural Circuitry. J Neurosci 40:JN-RM-2158-19.